From the nucleus to the plasma membrane: translocation of the nuclear proteins histone H3 and lamin B1 in apoptotic microglia

Barbara Klein[1,2,3], Ursula Lütz-Meindl[1], and Hubert H. Kerschbaum[1]

[1]Department of Cell Biology, University of Salzburg, Hellbrunnerstraße 34, A-5020 Salzburg, Austria

[2] Institute of Molecular Regenerative Medicine, Paracelsus Medical University, Strubergasse 21, A-5020 Salzburg, Austria

[3]Spinal Cord Injury and Tissue Regeneration Center Salzburg (SCI-TReCS), Paracelsus Medical University, Strubergasse 21, A-5020 Salzburg, Austria

Keywords: Apoptosis, microglia, histone, lamin, ultrastructure

Corresponding authors:

	Barbara Klein
Email address:	Barbara.klein@pmu.ac.at
Telephone number:	0043/662/8044/5592
Fax number:	0043/662/8044/619

	Hubert H. Kerschbaum
Email address:	Hubert.kerschbaum@sbg.ac.at
Telephone number:	0043/662/8044/5667
Fax number:	0043/662/8044/180

Abstract

Nuclear autoantibodies have been found in patients with autoimmune diseases. One possible source for nuclear antigens are apoptotic cells. However, the mechanism of how apoptotic cells make nuclear factors accessible to the immune system is still elusive. In the present study, we investigated the redistribution of nuclear components after UV irradiation in the microglial cell line BV-2 and in primary mouse microglia at the ultrastructural level. We used transmission electron microscopy (TEM)-coupled electron energy loss spectroscopy (EELS) to measure phosphorus as an indicator for nucleic acids and immunogold labeling to detect histone H3 and lamin B1 in apoptotic cells. EELS revealed elevated concentrations of phosphorus in nuclear and cytoplasmic condensed chromatin compared to the remaining cytoplasm. Furthermore, immunolabeling of lamin B1 and histone H3 was detected in apoptotic microglia not only in the nucleus, but also in the cytoplasm, and even at the plasma membrane. Confocal images of apoptotic microglia, which were not previously permeabilized, showed patches of histone H3 and lamin B1 labeling at the cell surface. The pan-caspase inhibitor Z-VAD-FMK (carbobenzoxy-valyl-alanyl-aspartyl-[O-methyl]-fluoromethylketone) prevented the occurrence of cytoplasmic condensed chromatin in apoptotic microglia. Our findings indicate that nuclear components leak from the nucleus into the cytoplasm in apoptotic microglia. At least histone H3 and lamin B1 reach the cell surface, this may promote autoreactive processes.

Introduction

Structural changes of the cell nucleus are prominent during apoptosis. Thus, classical hallmarks of apoptosis include condensation of chromatin at the nuclear periphery and fragmentation of the nucleus into membrane-enclosed particles [1], as well as DNA fragmentation and caspase-mediated cleavage of proteins of the nuclear lamina and nuclear envelope [2-5]. Additionally, it has been shown that nuclear proteins, usually sequestrated within the cell, are exposed in dying and dead cells (for example [6,7]). This makes apoptotic cells a potential source for nuclear antigens which may elicit autoimmune responses. However, under normal conditions, apoptotic cells are rapidly cleared by phagocytes (for a review see [8]). Only if this protective mechanism fails, it is possible that exposed nuclear antigens become accessible to immune cells, and, thus, may cause autoimmune reactions. In accordance with this hypothesis, an association between an impairment of phagocytosis and autoimmunity has been described [9-14]. While it is well established that apoptotic cells can deliver nuclear antigens to their microenvironment, the cellular mechanisms of extrusion of nuclear components are less understood.

Autoantibodies to nuclear proteins have been identified in autoimmune diseases like systemic lupus erythematosus (SLE) [15-17], in which also the central nervous system (CNS) is frequently affected [18,19]. Furthermore, antinuclear antibodies have been detected in patients suffering from in multiple sclerosis (MS), which primarily targets the CNS [20-27]. However, the role of these autoantibodies in the disease course of MS is still unclear [27,26]. Also for Alzheimer's disease and vascular dementia, there are reports of elevated serum titers of antihistone autoantibodies [28] or antinuclear autoantibodies [29]. For the present study, we chose to investigate microglia, an immune cell type that is abundantly present in the CNS.

Microglia are the endogenous tissue macrophages of the CNS and derive from primitive myeloid progenitors which arise before definitive hematopoiesis in the yolk sac [30]. The microglia population of the CNS is long-lived and not dependent on the infiltration of monocytes from the blood (reviewed in e.g. [31,32]). Under physiological conditions, microglia are in a so-called "resting" state, which entails, however, an active immune surveillance of their microenvironment. Following inflammatory or pathogenic stimuli, microglia change from surveillance to a reactive state [33]. Activated microglia can promote regenerative processes, e.g. by removing cell debris and by releasing neuroprotective factors,

or contribute to neurodegeneration by exacerbating inflammation (for reviews on microglial functions see e.g. [34,35,33]. Therefore, the beneficial or detrimental contribution of microglia to neuropathologies is still highly under debate and probably context-dependent (see for example [36-39]).

Activation of microglial cells is accompanied by a local increase in cell number, due to migration and proliferation, whereas down-regulation after an immune response may be associated with apoptosis [40-44]. In acute experimental autoimmune encephalomyelitis (EAE) and in chronic relapsing EAE, apoptotic microglial cells have been detected [45-47]. Even though microglia are facultative antigen-presenting cells, antigen presentation in the CNS does not usually occur in the CNS parenchyma, but, instead, in the perivascular space, the meninges and the choroid plexus (reviewed in [48]). CNS antigens exit the brain via the interstitial fluid to the cerebrospinal fluid (CSF) and from there to cervical lymph nodes, where these antigens can prime T cells, which, in turn, can travel the CSF (reviewed in [48]). If autoimmune memory T cells are restimulated on this route by CNS-endogenous antigen presenting cells, this may contribute to the pathogenesis of autoimmune diseases like MS [49,50].

Interestingly, immunofluorescence studies on apoptotic cells revealed the presence of nuclear proteins not only in the nucleus, but also in the cytoplasm and close to the plasma membrane in different cell types [51-55,7,56], suggesting an active export of chromatin from the nucleus to the cell periphery. Although these studies visualized nuclear proteins outside the nucleus on a light microscopic level, it was not examined whether these nuclear components were still contained within the nuclear envelope or not. Previously, we described in an electron microscopy study in the microglial cell line BV-2 chromatin-like material in the cytoplasm, which was not surrounded by a nuclear envelope [57]. Although we were able to identify these electron-dense patches morphologically as chromatin, we did not know their molecular composition.

Therefore, the aim of the present study was to characterize the nuclear components which are extruded into the cytoplasm in apoptotic microglia, in particular, we compared cells of the microglial cell line BV-2 with primary mouse microglia. For a detailed description of the apoptotic nuclear morphology in microglial cells, we combined the high spatial resolution of transmission electron microscopy with immunogold labeling and electron energy loss

spectroscopy (EELS) for the detection of phosphorus within the sample, as an indicator for nucleic acids. To exclude possible artifacts due to the method of tissue preparation for electron microscopy, we compared conventional chemical fixation with high pressure freeze fixation, in which the sample is frozen within milliseconds.

As a result, we localized at the ultrastructural level the core histone H3 and lamin B1, a component of the nuclear lamina, in condensed chromatin in the cytoplasm of apoptotic BV-2 microglia and primary mouse microglia. These nuclear proteins were also detected directly at the plasma membrane in both cell types. Furthermore, high levels of phosphorus, indicating the presence of nucleic acids, were identified in cytoplasmic condensed chromatin. We were able to inhibit the formation of cytoplasmic condensed chromatin patches with the pan-caspase inhibitor Z-VAD-FMK. Thus showing, that apoptotic microglial cells expose components of chromatin as well as of the nuclear lamina at their cell surface in a caspase-dependent way.

Materials and Methods

Chemicals

Most chemicals were bought from Sigma-Aldrich (Munich, Germany); exceptions are marked in the text.

Cell culture

Microglia from the mouse cell line BV-2 [58] and primary mouse microglia were cultivated at 95% relative humidity with 5% CO_2 at 37 °C. BV-2 cells were grown in Dulbecco's Modified Eagle's Medium (DMEM) containing 2200 mg glucose/l and 10% Fetal Calf Serum (FCS) (Biochrom, Berlin, Germany). Primary microglia were cultivated in DMEM (with 4500 mg glucose/l, L-glutamine, and pyruvate) (PAA Laboratories, Pasching, Austria) supplemented with 1% penicillin/streptomycin (Invitrogen, Paisley, UK) and 10% FCS. Primary microglia cultures were prepared from C57BL/6J mouse pups from P0 to P5 (modified after [59,60]). In short, after decapitation, cerebral cortices were isolated, and meninges and vasculature were carefully removed. The tissue was homogenized in cooled Hank's Balanced Salt Solution (HBSS) (Invitrogen, Paisley, UK) and, thereafter, incubated with trypsin (Invitrogen, Paisley, UK) at 37 °C for 25 min. After that, FCS and DNAse (2 mg/ml) (Fermentas, St. Leon-Rot, Germany) were added and the preparation was centrifuged. Next, the pellet was resupended in the cultivating medium, filtered through a 70 μm cell strainer (BD Biosciences, Schwechat, Austria) and the cells cultivated with a medium change after 24 h. After 1 to maximal 2 weeks, primary microglia were harvested by shaking the culture flasks for 3 h, and then the supernatants, containing >95% microglia, were collected. After that, primary microglia were cultivated for at least 12 h before the onset of experiments. For confocal laser scanning microscopy (CLSM), microglia were grown on poly-D-lysine-coated glass cover slips overnight; for other experiments cells were harvested directly from culture dishes.

Apoptosis induction

BV-2 and primary microglia were exposed to UV radiation (2500 J/m^2; 254 nm, Stratalinker 2400, Stratagene, La Jolla, CA, USA), and examined 1, 3, and 5 h after UV irradiation.

To investigate the influence of caspases on the morphological changes in apoptotic microglia, we used the pan-caspase inhibitor carbobenzoxy-valyl-alanyl-aspartyl-[O-methyl]-

fluoromethylketone (Z-VAD-FMK) (Promega, Mannheim, Germany). For this purpose, we started the incubation of cells with 20 µM Z-VAD-FMK 2 h before UV irradiation. As additional control, we examined cells incubated for 5 h with 20 µM Z-VAD-FMK without apoptosis induction.

Antibodies

Antibody staining with primary polyclonal rabbit IgG antibodies for lamin B1 (H-90) (Santa Cruz Biotechnology, Heidelberg, Germany) or histone H3 (H0164) were combined with CLSM or TEM. As secondary antibody for CLSM we used an Alexa Fluor 546 conjugated F(ab')$_2$ fragment of goat anti-rabbit IgG (H+L) (Invitrogen, Paisley, UK); for electron microscopy, we used an anti-rabbit IgG gold conjugate (10 nm).

CLSM

After the respective treatments, cells were fixed in 1% paraformaldehyde in phosphate-buffered saline (PBS) for 20 min. After fixation, cells were washed twice with PBS, then they were permeabilized with 0.2% Triton X-100 in PBS for 10 min. This step was left out for those experiments in which we wanted to test if the antigens were exposed at the plasma membrane surface. Next, the samples were blocked for 15 min in 3% normal goat serum (NGS) (PAA Laboratories, Pasching, Austria) in PBS, before incubation with the respective primary antibodies for 1 h at room temperature (for negative controls the primary antibodies were omitted). The anti-histone H3 antibody was diluted 1:300 in PBS with 3% NGS, the anti-lamin B1 antibody was diluted 1:400. After three washing steps, the samples were incubated for 20 min with the secondary antibody diluted 1:500 in PBS with 3% NGS. After washing steps, the samples were stained for 15 min with 4',6-Diamidino-2-Phenylindole (DAPI) in PBS (1:100), and then washed again. For image acquisition, we used a Leica TCS SP5 confocal laser scanning system (Mannheim, Germany), DAPI was excited with the 375 nm UV laser line, and Alexa Fluor 546 with the 561 nm laser line.

TEM

For TEM, cells were harvested using Trypsin EDTA (PAA Laboratories Company, Linz, Austria). In addition to chemical fixation (Fig. 1 A-E and Fig. 2-5,6), we also used high pressure freeze fixation (Fig. 1 F-I) providing best structural preservation due to its fast freezing rate of -10 °C/ms. This method excludes possible detrimental effects on the fixation quality induced by the comparably slow chemical fixation. Since the results we achieved with

high pressure freeze fixation were in accordance with what we observed in our chemically fixed samples, subsequent experiments were done using chemical fixation.

For chemical fixation, we used 1% glutaraldehyde in 50 mM cacodylate buffer for 15 min at room temperature, before postfixation at 4 °C over night in 2% osmium tetroxide (Electron Microscopy Sciences, Hatfield, UK) in 50 mM cacodylate buffer. After that, samples were dehydrated on ice in a graded ethanol series with an intermediate en-bloc staining step for 1 h in 2% uranyl acetate dihydrate (in 70% ethanol). After intermediate steps in propylene oxide, the samples were embedded in Agar Low Viscosity Resin (Agar Scientific, Stansted, UK), or, for immunocytochemical studies, directly in LR White Resin (London Resin Company, Berkshire, UK).

For high pressure freeze fixation, cells were frozen in a Leica EMPACT and freeze-substituted in a Leica EM AFS freeze substitution apparatus in acetone containing 2% OsO_4 and 0.05% uranyl acetate dihydrate. During substitution, the temperature was first -80 °C for 52.5 h, and then it was raised within 5 h to -30 °C, which was kept for 4 h. After that, the samples were warmed within 3.5 h to 5 °C for at least 5 h. After rinsing with acetone at room temperature, the samples were embedded in epoxy resin (modified after [61]).

Ultrathin sections were examined in a LEO 912 AB Omega transmission electron microscope (Carl Zeiss, Oberkochen, Germany) operated with a LaB_6 cathode and equipped with an in-column energy filter. For conventional imaging an acceleration voltage of 80 kV was used. Micrographs were taken with a Proscan dual slow-scan CCD camera (Proscan, Lagerlechfeld, Germany), a TRS sharp:eye camera controller (Tröndle Restlichtverstärkersysteme, Moorenweis, Germany), and iTEM software (Olympus Soft Imaging Solutions, Münster, Germany).

Immunogoldlabeling for TEM

Ultrathin sections mounted on gold grids were treated for 1 h with a blocking solution (2% bovine serum albumin, 0.1% Tween 20, 50 mM Trizma preset crystals, at pH 7.4), and incubated for 2 h with a primary polyclonal rabbit antibody for histone H3 (dilution 1:70 on LR White Resin for BV-2 cells, or 1:30 on Agar Low Viscosity Resin for primary microglia) or for lamin B1 (dilution 1:25) in blocking solution. After four washing steps, the sections were incubated for 30 min with a secondary anti-rabbit antibody conjugated with gold (dilution 1:100). Then the sections were washed again in blocking solution and finally rinsed

in distilled water. Histone H3 was detected on cells embedded in LR White Resin as well as in Agar Low Viscosity Resin (using a higher antibody concentration), whereas anti-lamin B1 staining worked better on cells embedded in Agar Low Viscosity Resin. Negative controls, in which the primary antibodies were omitted, confirmed the specificity of the labeling.

Quantification of immunogold labeling and statistical analysis

For the quantification of immunogold labeling, electron micrographs of randomly selected cell sections were taken at a magnification of 2,500x. The distribution of immunogold labeling was quantified by dividing cells in three compartments: (1) electron-dense areas of the nucleus, (2) cytoplasm including all organelles (with exception of phagosomes, autophagosomes and lysosomal structures) (3) plasma membrane. Then the number of gold particles per compartment was counted using ImageJ 1.45s (developed by Wayne Rasband, National Institutes of Health, USA; ImageJ website: http://imagej.nih.gov/ij/) with a Cell Counter Plugin (Kurt De Vos, University of Sheffield, UK; downloaded from http://rsbweb.nih.gov/ij/plugins/cell-counter.html), and the density of gold particles per area (of the nucleus or cytoplasm) or length (of plasma membrane) was calculated. For each condition and antibody, at least six cells, from three independent experiments, were analyzed this way.

Statistical analyses were done using IBM SPSS Statistics 20 software (IBM Corporation, Armonk, NY, USA). Independent samples t-tests were used for data comparison and the calculation of significance levels (p values of $p < 0.001$ (***) were considered most significant, $p < 0.01$ (**) highly significant, and $p < 0.05$ (*) significant). Data are depicted as mean plus standard deviation (s.d.).

EELS

For EELS measurements at the phosphorus K-edge, at an energy loss of 2173 eV, ultrathin sections (50 nm) mounted on uncoated copper grids were used. The transmission electron microscope was operated at an acceleration voltage of 120 kV with illumination angles of 2.5 or 3.15 mrad at magnifications of 25,000x or 50,000x. The exposure time was 50 s, and seven integration cycles were acquired for each measurement. The resulting graphs were filtered using the exact Blackman filter provided by the iTEM software.

DNA fragmentation analysis

DNA fragmentation analysis was performed 1, 3, and 5 h after apoptosis induction with a protocol modified from [62]. BV-2 cells were lysed with TE/Triton buffer (10 mM Tris-HCl, 20 mM EDTA, 0.5% Triton X-100, pH 8) for 20 min on ice, then the nuclei were removed by centrifugation (12 000 g for 10 min) and the supernatants were incubated with proteinase K (0.1 mg/ml) (Fermentas, St. Leon-Rot, Germany) with 0.5% sodium dodecyl sulfate for 1 h at 50 °C. The supernatants were extracted with chloroform-isoamylalcohol (24:1) at room temperature. Nucleic acids were precipitated with 0.1 volumes 3 M sodium acetate and 2.5 volumes ethanol (on ice) for 30 min at -80 °C. After centrifugation, the pellets were washed with 70% ethanol, dissolved in double distilled water, incubated with RNase A (250 µg/ml) (Fermentas, St. Leon-Rot, Germany) for 1 h at 37 °C, and analyzed by agarose gel electrophoresis.

Results

Condensed chromatin is found in the cytoplasm of apoptotic microglia

Primary mouse microglia and cells of the microglial cell line BV-2 were irradiated with UVC to induce apoptosis, and after 1, 3 or 5 h, processed for TEM. To preserve the ultrastructure as closely as possible to the native state, we used, in addition to chemical fixation (Fig. 1A-E), high pressure freeze fixation (Fig. 1F-I). Although DNA fragmentation, analyzed by agarose gel electrophoresis, was detectable already within 1 h after UV irradiation in BV-2 cells (Suppl. Fig. 1), the ultrastructure of the nucleus (Fig. 1G) did not differ from control cells (Fig. 1A,F). At later stages, apoptotic BV-2 microglia were characterized by classical condensed chromatin accumulation at the nuclear periphery (Fig. 1B-E, H-I).

Additionally, we identified electron-dense structures resembling condensed chromatin in the cytoplasm of apoptotic BV-2 cells (Fig. 1B-E, H). These cytoplasmic chromatin patches were detected in chemically fixed (Fig. 1B-E) as well as in high pressure frozen BV-2 cells (Fig. 1H). Because high pressure freezing takes place with a freezing rate of -10 °C/ms, we assume that cytoplasmic condensed chromatin is a genuine feature of apoptosis induced by UV irradiation in mouse microglia, and not an artifact due to fixation. Cytoplasmic condensed chromatin patches varied in size, location, and shape, e.g. spherical (Fig. 1C) or irregularly shaped (Fig. 1B, H). Surprisingly, these patches of nuclear material were never enclosed by a double or single membrane. The largest patches of cytoplasmic chromatin reached a diameter of several micrometers. These cytoplasmic chromatin patches were often found densely concentrated in certain areas adjacent to the nuclear envelope, suggesting that chromatin leaks from the nucleus at focal release sites (Fig. 1B-C). Although cytoplasmic condensed chromatin was widely distributed throughout apoptotic cells, the nuclear envelope was still present and seemed morphologically intact. This suggests that the extrusion of condensed chromatin is not due to a disintegration of the nuclear envelope. Nevertheless, the structure of the nuclear envelope deviated from healthy cells. In apoptotic BV-2 cells, the nuclear envelope was dilated, the outer nuclear membrane showed protrusions, and the nucleus was surrounded by numerous vesicles (Fig. 1C, I). Within the cytoplasm, mitochondria appeared to be attractors of cytoplasmic condensed chromatin (Fig. 1D-E). Moreover, we detected cytoplasmic condensed chromatin at the plasma membrane region (Fig. 1B).

Cytoplasmic nuclear components contain phosphorus, histone H3, and lamin B1

To evaluate the similarities between nuclear and cytoplasmic electron-dense chromatin patches, we used EELS to quantify phosphorus as an indicator for nucleic acids and immunogold labelling to localize the nuclear proteins histone H3 and lamin B1.

EELS measurements detected the relative amount of electrons of the primary electron beam which lost energy at the phosphorus K-edge (at 2173 eV) while passing through the sample. Figure 2 shows representative EELS measurements at the phosphorus K-edge at different cellular locations. In control BV-2 cells, the only areas where a phosphorus peak was detectable were electron-dense areas of chromatin within the nucleus (Fig. 2A). In apoptotic BV-2 cells, EELS measurements were taken in areas containing condensed chromatin within the nucleus, in the cytoplasm where we morphologically identified chromatin, in other cytoplasmic areas, as well as in the embedding material (Fig. 2B). High levels of phosphorus were found in nuclear as well as in cytoplasmic condensed chromatin. In areas of the cytoplasm without condensed chromatin and in the embedding medium the amount of phosphorus was below detection. These measurements indicate that the morphologically distinguishable cytoplasmic condensed chromatin contains a phosphorus-rich material, presumably nucleic acids.

To further investigate the composition of cytoplasmic nuclear material we did immunogold labeling for TEM analysis using polyclonal antibodies to histone H3 or lamin B1. In control BV-2 cells, the antibody labeling of histone H3 was concentrated within the nucleus (Fig. 3A). In apoptotic cells, dense histone H3 labeling was found in chromatin within the nucleus as well as in patches of cytoplasmic condensed chromatin (Fig. 3B). Histone H3 labeling was not restricted to structurally identifiable cytoplasmic condensed chromatin, but was distributed throughout the cytoplasm and even found at the region of the plasma membrane (Fig. 3C). This may indicate that cytoplasmic condensed chromatin is further processed in the cytoplasm leading to the exposure of histone H3 at the plasma membrane.

Ultrastructural analysis of immunogold labeling with a polyclonal lamin B1 antibody revealed labeling within the nucleus of control BV-2 cells (Fig. 3D). In apoptotic BV-2 cells, lamin B1 labeling was additionally found in patches of nuclear material in the cytoplasm (Fig. 3E). Interestingly, vesicles close to the nuclear envelope were also detected by the lamin B1 antibody (Fig. 3E). This could indicate that these vesicles derived from the nuclear envelope.

Quantitative analysis of the distribution of immunogold particles in BV-2 microglia after staining with histone H3 or lamin B1 antibodies confirmed these observations (Fig. 3F-H). In comparison to controls, apoptotic BV-2 cells had a significantly higher labeling density in the cytoplasm after immunogold staining of histone H3 (Fig. 3F) or lamin B1 (Fig. 3G). Also, labeling directly at the plasma membrane was significantly increased with both antibodies in apoptotic cells (Fig. 3H). There was also an increase in labeling in the electron-dense areas of the nucleus in apoptotic microglial cells. This could be explained by the shrinkage of the nucleus during apoptosis which is accompanied by a condensation of nuclear components, which would increase the labeling density per area.

In primary mouse microglia, we found basically the same results as in cells of the microglial cell line BV-2 after UV irradiation (Fig. 4 and 5). Unlike control cells (Fig. 4A), apoptotic primary microglia had condensed chromatin patches in the cytoplasm (Fig. 4B-C), although they tended to be smaller and more spherical than in BV-2 microglia. Additionally, the nuclear envelope was dilated in apoptotic primary microglia (Fig. 4D). Moreover, also in primary microglia, immunogold labeling of histone H3 was concentrated within the nucleus in control cells (Fig. 5A), and in cytoplasmic patches of nuclear material in apoptotic cells (Fig. 5B-C), and lamin B1 staining showed a similar distribution pattern (Fig. 5 D-F). A quantification of the immunogold labeling showed a significant increase of histone H3 and lamin B1 in the cytoplasm (Fig. 5G-H) and directly at the plasma membrane (Fig. 5I) of apoptotic primary microglia in comparison to controls.

Caspase-dependent translocation of nuclear components

To evaluate whether caspase activity is associated with the extrusion of nuclear components into the cytoplasm, BV-2 microglia were treated with the pan-caspase inhibitor Z-VAD-FMK (20 µM) starting 2 h before UV irradiation. Three hours after UV irradiation, cells were chemically fixed and processed for TEM. The morphology of BV-2 microglia treated for 5 h with 20 µM Z-VAD-FMK alone closely resembled control conditions (Fig. 6A). Despite pretreatment with Z-VAD-FMK, BV-2 cells showed chromatin condensation after UV irradiation, however, cytoplasmic condensed chromatin was not detectable in these cells (Fig. 6B-C). Additionally, caspase inhibition blocked dilation of the nuclear envelope, whereas formation of apoptotic bodies was not affected. Moreover, UV-irradiated cells pretreated with Z-VAD-FMK showed a much higher volume of both cell and nucleus in comparison to cells only exposed to UV irradiation (Fig. 6B-C).

Using CLSM, we were able to reproduce our TEM findings of the UV-induced redistribution of histone H3 and lamin B1 in BV-2 cells (Fig. 7A-D) and in primary microglia (Fig. 7E-H). Additionally, we investigated whether labeling with histone H3 and lamin B1 antibodies was also detectable in primary microglia, which were not previously permeabilized. In contrast to non-permeabilized control cells, in which hardly any histone H3 labeling was detectable (Fig. 7I), patches of histone H3 labeling at the cell surface were visible in non-permeablized apoptotic BV-2 microglia 3 hours after UV irradiation (Fig. 7J). Labeling of lamin B1 without permeabilization yielded the same results in control primary microglia (Fig. 7K) and in UV-irradiated primary microglia (Fig. 7L).

Our study demonstrates a Z-VAD-FMK-inhibitable translocation of nuclear material to the cytoplasm in apoptotic microglia. The presence of histone H3 or lamin B1 on the cell surface may promote autoreactive processes.

Discussion

Extrusion of nuclear components happens early during microglial apoptosis

In the present study, we used UVC irradiation to induce apoptosis, which almost exclusively leads to DNA damage (for a review see [63]). In a previous study [57], we demonstrated that this treatment induces in BV-2 microglia a strong caspase 3/7 activity already after 3 h, with no significant further increase after 6 h. A quantification of Annexin V-positive/propidium iodide-negative cells yielded a similar result, i.e. already 3 h after UVC irradiation more than 50% cells are Annexin V-positive (and PI-negative), a number which is not significantly further increased after 6, 9 and 12 h. Furthermore, an investigation of nuclear morphology using DAPI staining revealed that 6 h after UVC irradiation already more than 70% nuclei showed clearly detectable changes in their morphology ("early stages") and 25% a strongly collapsed nuclear structure ("late stages") [57]. Based on these results, we limited our present study to 3 and 5 h after apoptosis induction via UVC irradiation, to investigate time points in which apoptotic changes of the nucleus were still ongoing and to exclude "late stages" of nuclear morphology. Therefore, we propose that the observed extrusion of nuclear components is an early process during apoptosis in microglia.

Irrespective of the fixation method, we observed condensed chromatin in the cytoplasm and at the plasma membrane of BV-2 cells and of primary mouse microglia during UVC-induced apoptosis – even though the nuclear envelope was morphologically still intact. Even earlier, i.e. before condensed chromatin was found in the cytoplasm, its degradation was already detectable as DNA laddering (Suppl. Fig. 1). A more detailed analysis of the extruded nuclear material showed that it not only contained chromatin (as evidenced by the detection of the core histone H3) as well as high phosphorus levels indicative of the presence of nucleic acids, but also lamin B1 which is a component of the nuclear lamina. Although, early apoptotic changes in primary microglia and BV-2 cells include a dilation of the nuclear envelope and an increase in vesicle formation at the outer membrane of the nuclear envelope, we did not observe endocytosis-like structures at the inner membrane of the nuclear envelope, nor vesicles containing electron-dense material between the double membranes of the nucleus. Also, the nuclear material in the cytoplasm was not contained within a membrane, and seemed to accumulate close to the nucleus at focal release sites. For these reasons, we postulate that chromatin and parts of the nuclear lamina are first degraded and then might leave the nucleus via the nuclear pores by caspase-mediated processes. In accordance with

this hypothesis, an increase in permeability despite a morphologically intact nuclear envelope has been described in some studies as an early apoptotic event [64,65] and also during calcium-mediated cell death [66]. A report by Frisoni and colleagues [52] shows an involvement of caspases in the translocation of nuclear components. This study demonstrated that in a mouse model that lacks caspase-activated DNAse (CAD), and, thus, has no chromatin and nuclear fragmentation during apoptosis, the release of chromatin from cells during apoptosis is inhibited, and lupus autoimmunity to chromatin and other nuclear factors is reduced [52]. This data, together with our finding that the extrusion of nuclear components is suppressed by the pan-caspase inhibitor Z-VAD-FMK, and reports showing a proteolysis of nuclear pore proteins by caspases [67] suggest a caspase-dependent dilation of nuclear pores in apoptotic cells permitting the translocation of larger molecules than in intact cells.

Is translocation of nuclear components a general feature of apoptosis?

During apoptosis, nuclear proteins and DNA have been identified in the cytoplasm of several cell types using light microscopy. For example, in UVB-irradiated or staurosporine-exposed human keratinocytes and lymphoblasts, it was shown that apoptotic blebs contain nucleosomal DNA, nuclear ribonucleoproteins and histones [6]. Nucleosomes were also identified at the cell surface of apoptotic Jurkat cells after treatment with camptothecin or anti-Fas antibody [7], and nucleosomes and core histones were found in the cytoplasm of apoptotic lymphoblasts [53]. Nuclear factors in the cytoplasm may even enhance apoptotic processes, since it was shown that histone H1.2 is not only redistributed in mouse thymocytes during apoptosis induced by DNA double-strand breaks, but also involved in Bak-mediated release of cytochrome *c* from mitochondria [54]. Moreover, a co-localization of histone H1.2 with Bak in mitochondria was also found in bleomycin-treated human squamous carcinoma SCCTF cells [55]. Our observation that some mitochondria are surrounded by cytoplasmic condensed chromatin in apoptotic cells is in agreement with this finding. Interestingly, it was shown *in vitro* that histones (H1, H2A, H2B, and H3) are released from damaged adult CNS tissue, and that histone H1 is neurotoxic and able to activate microglial cells [68].

In summary, these findings strongly indicate that nuclear material does not stay concealed in the nucleus after different modes of apoptosis induction.

Is the extrusion of nuclear components in apoptotic microglia similar to NETosis?

Another mechanism by which nuclear proteins could become targets of autoimmune reactions is the formation of neutrophil extracellular traps (NETs) (reviewed in [69-71]), a process in which a filamentous net of DNA containing anti-microbial proteins, like histones, is extruded from cells and used to trap pathogens (for reviews about NET formation see [72,73,70,74,75]). NETosis was first discovered in neutrophils [76], but has also been described in other immune cell types (reviewed in [74]) like eosinophils (reviewed in [77]), mast cells [78] and macrophages [79-83]. NETs and the nuclear material which is extruded from apoptotic microglial cells have a similar molecular composition, since both consist of nucleic acids and histones. Histones, especially H3 and H4, have bactericidal properties ([84]; reviewed in [85]). Therefore, it seems plausible that the extrusion of nucleic material from apoptotic microglia could have a comparable immunological function as the formation of NETs. However, there are some notable differences between these two processes. While we observed classical apoptotic features in microglial cells in our study, NETosis is characterized by a different ultrastructural morphology in which chromatin is decondensed and both the nuclear envelope as well as the plasma membrane disintegrate (for example see [86,87,76]. Other apoptotic hallmarks, which we observed in UV-irradiated microglial cells, were phosphatidylserine exposure [57] and DNA fragmentation (Suppl. Fig 1), however, neither of those are features of NETosis (for reviews see ([74,75]). Also, the volume of the extruded nuclear material is much smaller in microglial cells than what is described in neutrophils (for example [76,87] or macrophages ([79-81]). Surprisingly, it has been shown in eosinophils [88] and neutrophils [89], that the DNA building the underlying structure of NETs can also be derived from mitochondria [88,89]. This is especially interesting, since in our study we observed a close spatial association between mitochondria and electron-dense nuclear material, and we cannot exclude the possibility that at least part of this electron-dense material is derived from these organelles themselves. Also, some of the high phosphorus content we observed in this electron-dense material could be derived from extruded mitochondrial DNA. In summary, it is possible that, despite their different morphology, the extrusion of nuclear material from apoptotic microglial cells and NET formation may have similar immunological functions. To clarify this issue, further studies about the pathways leading to the extrusion of nuclear material in microglia and a detailed analysis of potential anti-microbial effects of the extruded material would be necessary.

Possible link between apoptosis and the development of autoimmune diseases

While opsonization of apoptotic cells with autoantibodies against nuclear antigens can stimulate phagocytosis by dendritic cells [51], an impairment of phagocytosis may be involved in the formation of antinuclear antibodies in autoimmune diseases [9-13]. Thus, if apoptotic cells exposing nuclear factors on their cell surface are not rapidly cleared by phagocytes, this may trigger the generation of antinuclear antibodies, which are well characterized in SLE [17,15,16], but also detectable in other autoimmune diseases, like MS [22,20,21,23]. For example, in a subset of patients with SLE, high titers of autoantibodies to lamin B1 were observed [90]. In a follow-up study, apoptosis was induced in Jurkat and endothelial cells with anti-FAS antibody or staurosporine. In this study, it was confirmed that lamin B1 is indeed redistributed from the nuclear lamina to apoptotic blebs, however, not exposed at the cell surface, since it was not detected with CLSM using anti-lamin antibodies and aLB1 derived from SLE patients [91]. In contrast, it was shown that lamin B1 is exposed on the surface of apoptotic neutrophils [92], and furthermore, we were able to detect lamin B1 at the surface of apoptotic microglia, suggesting, that the exact composition of the extruded nuclear components may be cell type-dependent.

Our present study demonstrates a caspase-dependent extrusion of histone H3 and lamin B1 from apoptotic microglia *in vitro*, and, even though, it is intriguing to speculate that this process could play a physiological role for the innate immune system (similar to the formation of NETs), or (under conditions in which phagocytosis fails) could be relevant for the pathogenesis of autoimmune diseases, the implications of these findings still have to be studied in detail *in vivo*.
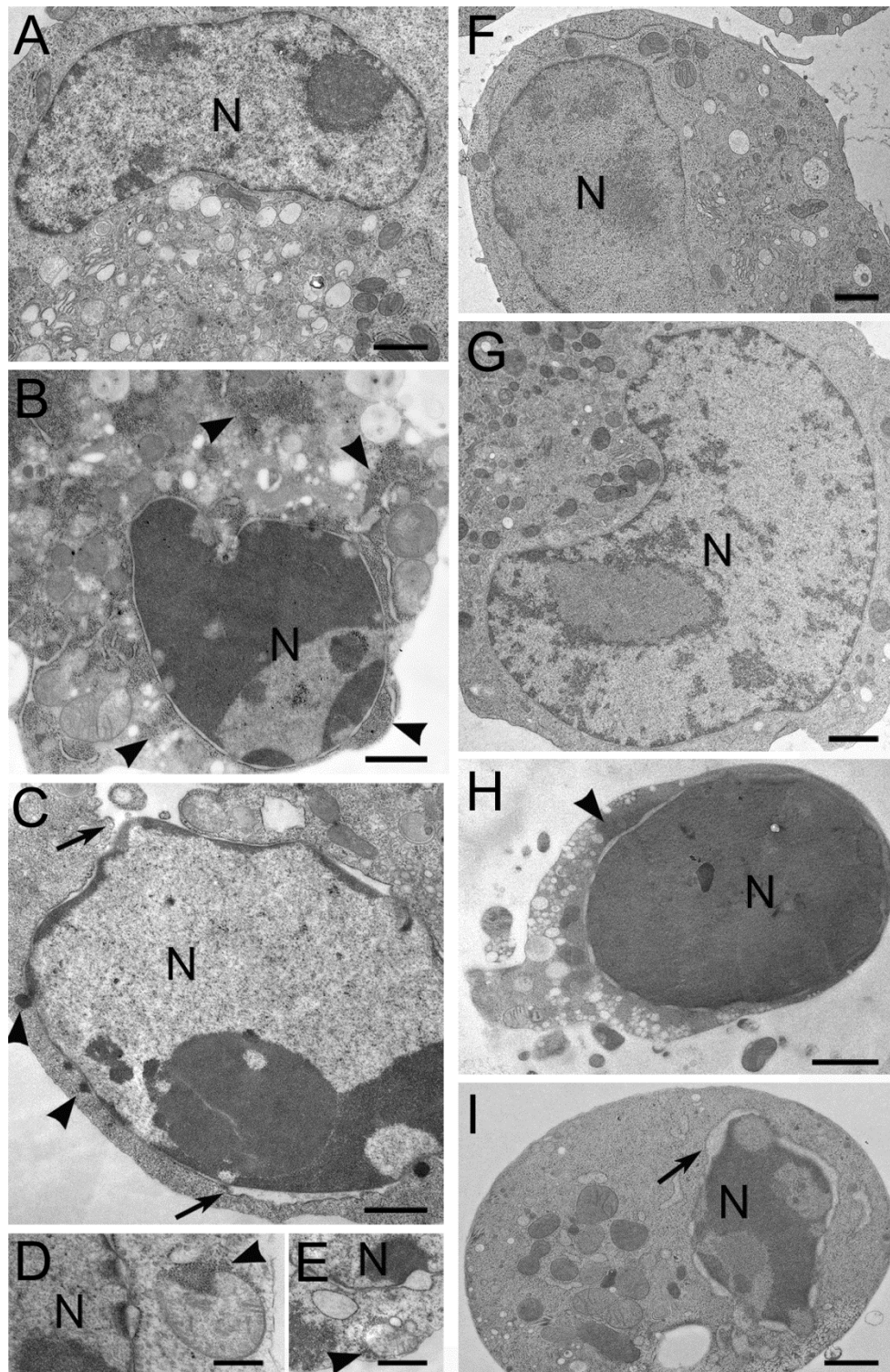
Acknowledgements

Figures

Fig. 1

Fig. 1 UV-induced changes in the ultrastructure of BV-2 microglia after chemical fixation (A-E) and high pressure freeze fixation (F-I). (A) Chemically fixed control cell. The nucleus is indicated (N). (B-E) Chemically fixed BV-2 cells 3 h after UV irradiation with condensed chromatin within the nucleus (N), cytoplasmic condensed chromatin patches

(arrowheads), and a dilated nuclear envelope (arrows). (D-E) Mitochondria surrounded by cytoplasmic condensed chromatin (arrowheads). (F) High pressure-frozen control BV-2 cell. The nucleus is indicated (N). (G) High pressure-frozen BV-2 cell 1 h after UV irradiation. Ultrastructure is similar to control conditions. (H-I) High pressure-frozen BV-2 cells 3 h after UV irradiation with condensed chromatin in the nucleus (N) and in the cytoplasm (arrowhead) and a dilated nuclear envelope (arrow). All bars 1 μm.
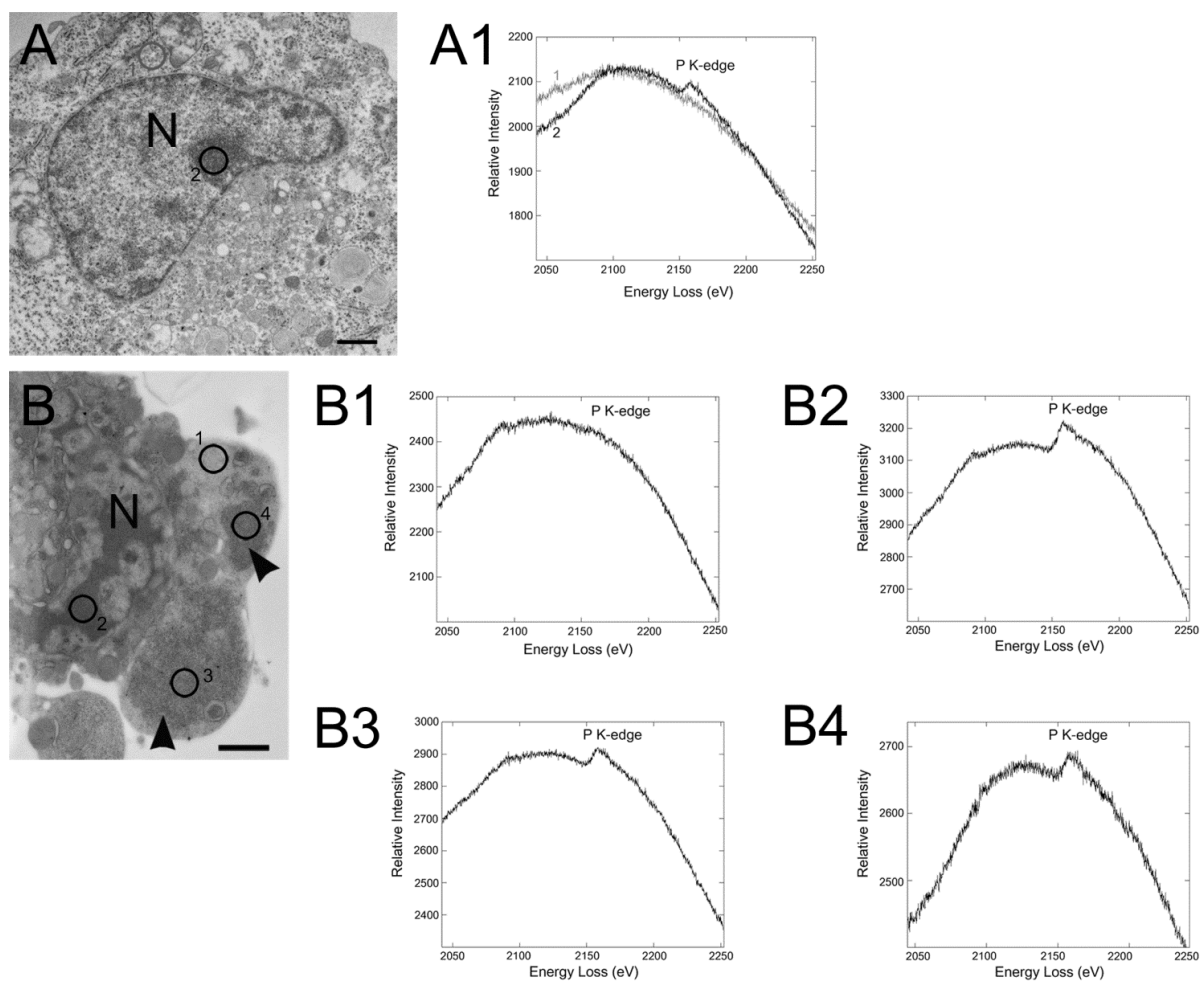
Fig. 2

Fig. 2 Redistribution of phosphorus-rich material during apoptosis in BV-2 microglia measured by electron energy loss spectroscopy (EELS) at the phosphorus K-edge (2173 eV). (A) Control BV-2 cell. Circles indicate measurement areas of EEL spectra in A1. (A1) Representative EEL spectra of measurements taken (1) in the cytoplasm where no peak at the P K-edge was detectable and (2) at an area of electron-dense chromatin within the nucleus (N), where a P K-edge peak was detected. (B) Apoptotic BV-2 cell 3 h after UV irradiation. (B1) EELS measurement in an area of the cytoplasm without chromatin. No peak at the P K-edge was detectable. (B2) EEL spectrum of an area which contains condensed chromatin within the nucleus. A phosphorus peak is clearly visible. (B3-4) EELS measurements taken at areas of the cytoplasm in which chromatin can be morphologically distinguished. P K-edge peaks are detectable. All bars 1 μm.
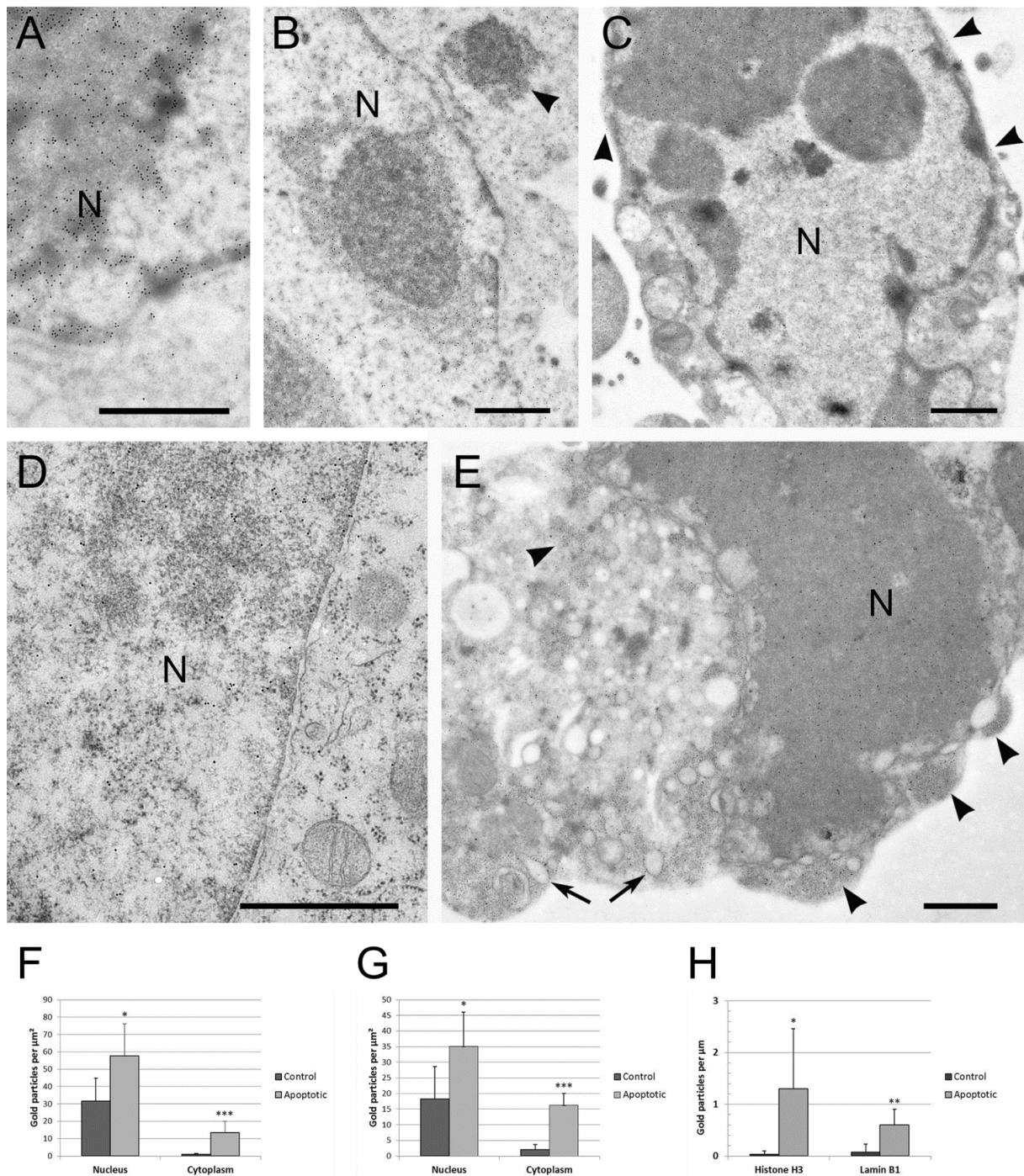
Fig. 3

Fig. 3 Immunogold labeling of histone H3 and lamin B1 in BV-2 microglia. (A-C) BV-2 microglia labeled with a polyclonal antibody for histone H3. (A) Control BV-2 cell. Histone H3 labeling is concentrated within the nucleus (N). (B-C) Apoptotic BV-2 cells 3 h after UV irradiation. (B) Dense labeling of histone H3 is not only found within the nucleus (N), but also in a cytoplasmic condensed chromatin patch (arrowhead). (C) Histone H3 labeling is also

found at the plasma membrane region (arrowheads). (D-E) BV-2 microglia labeled with a polyclonal anti-lamin B1 antibody. (D) Control BV-2 cell. Lamin B1 labeling is mainly found within the nucleus. (E) Apoptotic BV-2 cell 3 h after UV irradiation. Lamin B1 labeling is found densely concentrated within cytoplasmic condensed chromatin (arrowheads), as well as at the plasma membrane region, and on vesicles in the vicinity of the nucleus (arrows). All bars 1 μm. (F-H) Quantification of immunogold labeling in BV-2 microglia. (F) In apoptotic BV-2 cells, there is significantly more histone H3 detectable the electron-dense areas of the nucleus as well as in the cytoplasm of apoptotic cells compared to controls. (G) Lamin B1 density not only increases in the electron-dense areas of the nucleus, but is also significantly higher in the cytoplasm of apoptotic BV-2 cells in comparison to controls. (H) Histone H3 as well as lamin B1 labeling directly at the plasma membrane are significantly increased in apoptotic BV-2 cells in comparison to controls. Statistical analysis was done using independent-samples t-tests. Significance values were calculated in relation to control conditions (***$p<0.001$, **$p<0.01$, *$p<0.1$). The results are shown as mean + s.d.
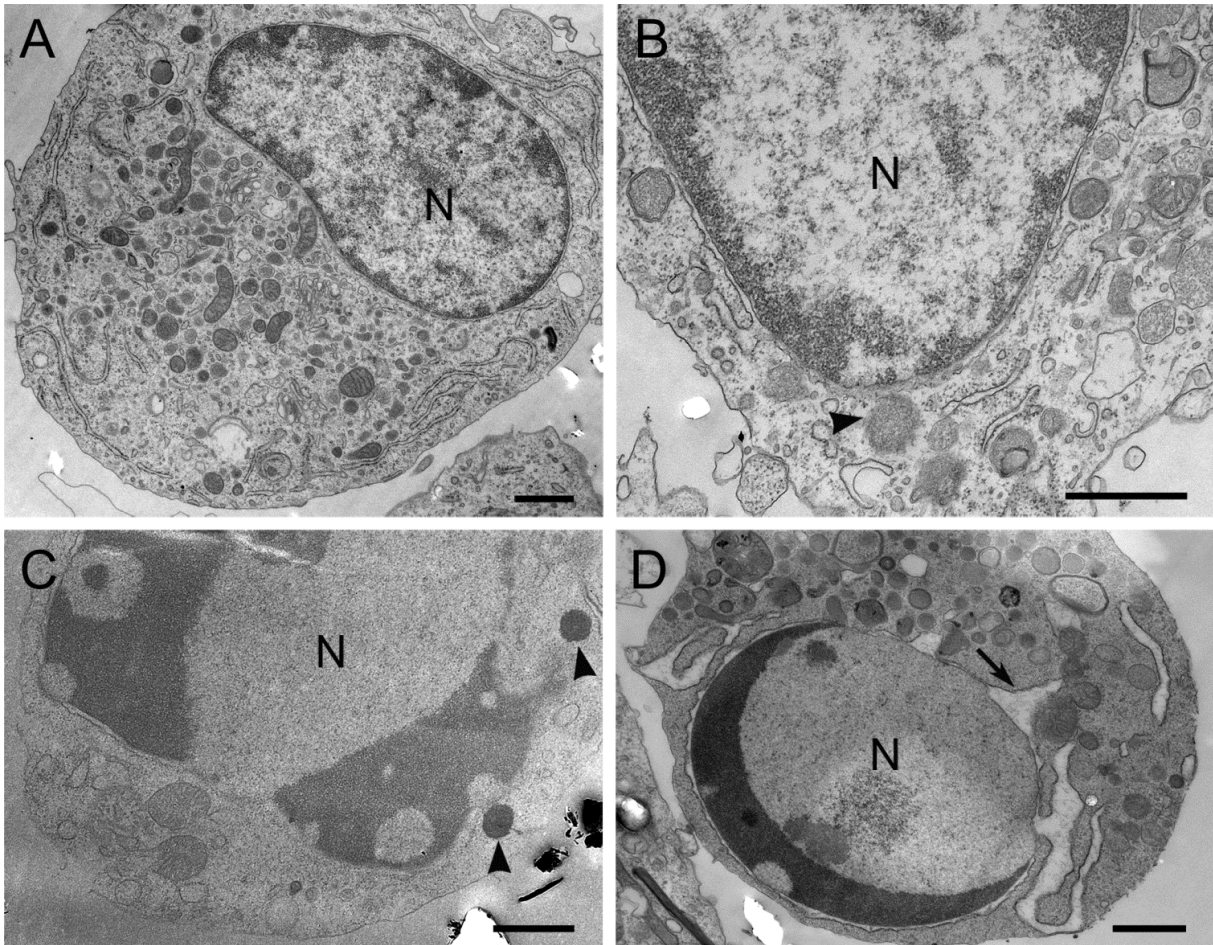
Fig. 4 UV-induced changes in primary mouse microglia. (A) Control cell. Nucleus is indicated (N). (B-D) Primary mouse microglia 3 h after UV irradiation. (B) Early apoptotic cell with a patch of cytoplasmic condensed chromatin (arrowhead). (C-D) Late apoptotic cells with condensed chromatin within the nucleus (N), cytoplasmic chromatin patches (arrowheads) and a dilated nuclear envelope (arrow). All bars 1 μm.
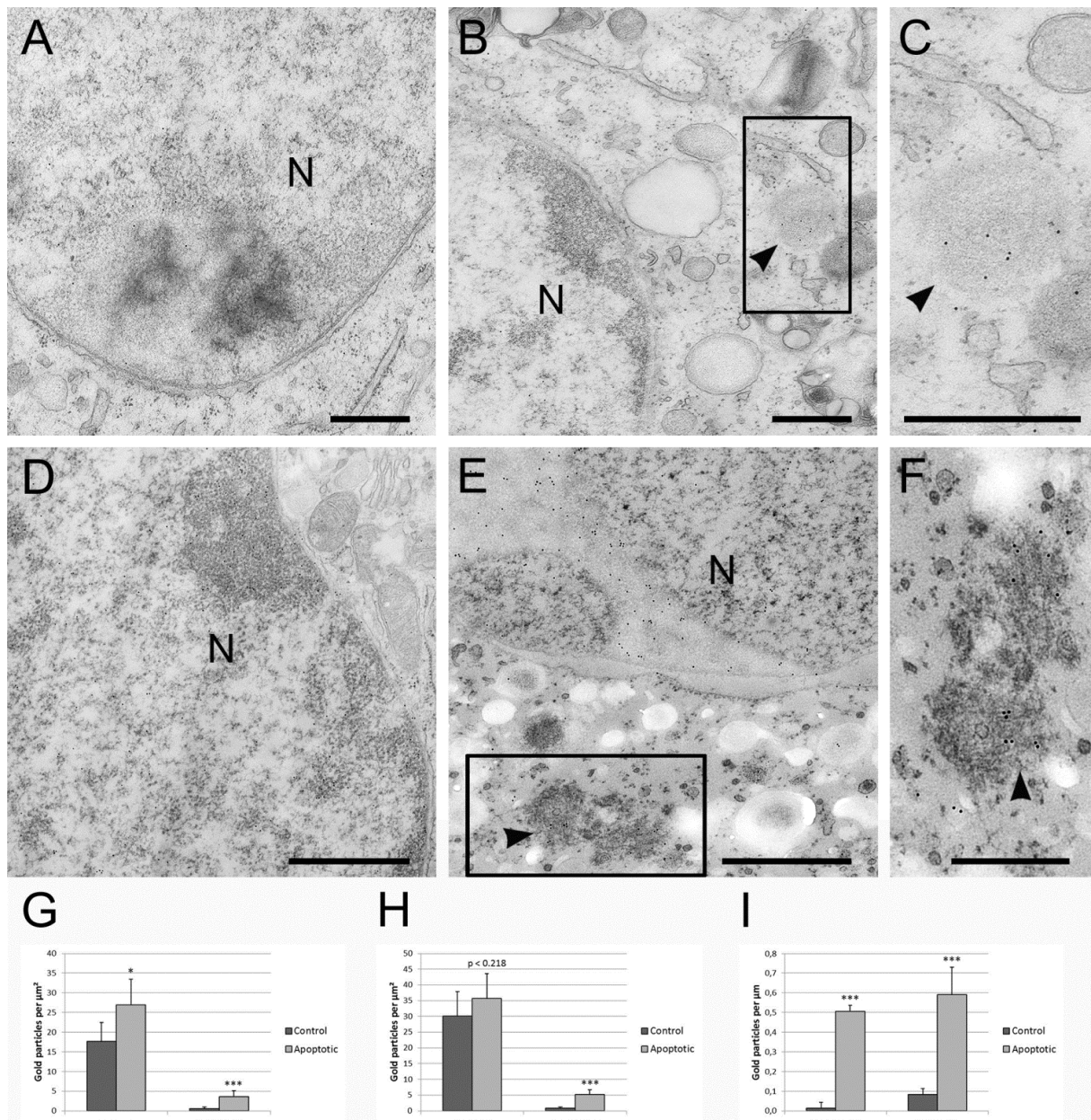
Fig. 5 Immunogold labeling of histone H3 and lamin B1 in primary mouse microglia. (A-C) Primary mouse microglia labeled with a polyclonal antibody for histone H3. (A) Control cell. Histone H3 labeling is found mainly within the nucleus (N). (B-C) Apoptotic cell 3 h after UV irradiation. The histone H3 antibody does not only label the nucleus (N), but also a roundly shaped cytoplasmic chromatin patch (arrowhead), which is magnified, as indicated by the rectangle, in (C). (D-F) Primary mouse microglia labeled with a polyclonal antibody for lamin B1. (D) Control cell. Lamin B1 labeling is concentrated within the nucleus (N). (E-F) Apoptotic primary mouse microglia 3 h after UV irradiation. Lamin B1 labeling is not only found within the nucleus (N), but also densely in a cytoplasmic chromatin patch (arrowhead).

The area indicated by the rectangle is magnified in (F). (A-C,F) Bars 0.5 µm. (D-E) Bars 1 µm. (G-I) Quantification of immunogold labeling in primary mouse microglia. (G) Histone H3 labeling is significantly increased not only in the electron-dense areas of the nucleus, but also in the cytoplasm of apoptotic primary microglia in comparison to controls. (H) Lamin B1 labeling is significantly increased in the cytoplasm of apoptotic primary microglia in comparison to controls, whereas there is no significant difference in the labeling density within the electron-dense areas of the nucleus (p<0.218). (I) At the plasma membrane, there is significantly more histone H3 as well as lamin B1 labeling in apoptotic primary microglia in comparison to controls. For statistical analysis independent-samples *t*-tests were used. Significance values are indicated in relation to control conditions (***p<0.001, **p<0.01, *p<0.1). The results are depicted as mean + s.d.
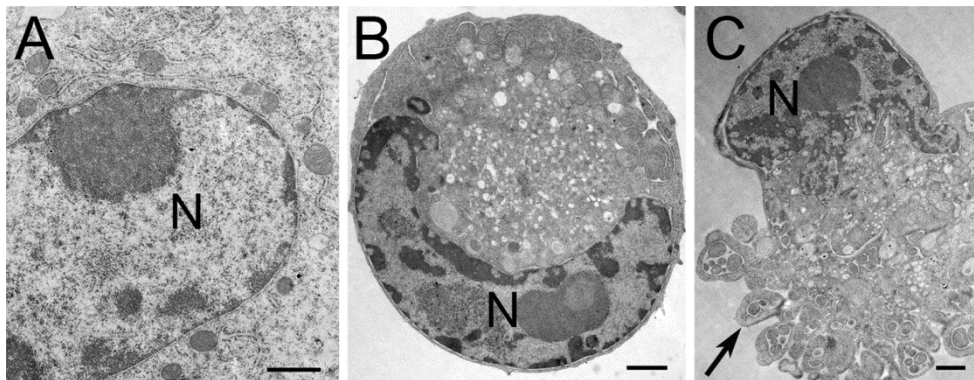

Fig. 6

Fig. 6 UV-induced chromatin extrusion and dilation of the nuclear envelope are suppressed by Z-VAD-FMK. (A) BV-2 cell treated with 20 µM Z-VAD-FMK for 5 h. Ultrastructure is similar to control conditions. (B-C) BV-2 cells incubated for 5 h with 20 µM Z-VAD-FMK and 3 h after UV irradiation. Although chromatin within the nucleus (N) was condensed, no chromatin was found in the cytoplasm. (C) Formation of apoptotic bodies (arrow) is not inhibited by Z-VAD-FMK.
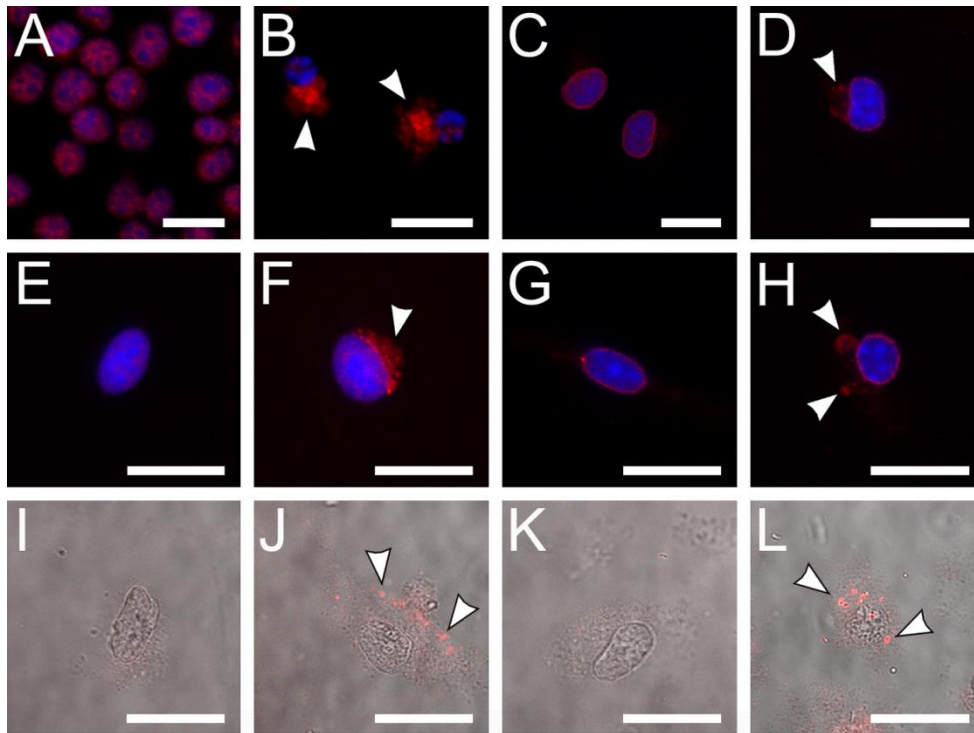
Fig. 7

Fig. 7 Confocal images of redistribution of histone H3 and lamin B1. (A) BV-2 control cells labeled with DAPI and anti-histone H3. (B) Apoptotic BV-2 cells labeled with DAPI and anti-histone H3. Histone H3 was also found within the cytoplasm (arrowheads). (C) Control BV-2 cells labeled with DAPI and anti-lamin B1. (D) Apoptotic BV-2 cell 3 h after UV irradiation labeled with DAPI and anti-lamin B1. Lamin B1 was also detected within the cytoplasm (arrowhead). (E) Control primary mouse microglia labeled with DAPI and anti-histone H3. (F) Primary mouse microglia 3 h after UV irradiation labeled with DAPI and anti-histone H3. Histone H3 was detected not only within the nucleus, but also in the cytoplasm (arrowhead). (G) Control primary mouse microglia labeled with DAPI and lamin B1. (H) Apoptotic primary mouse microglia labeled with DAPI and anti-lamin B1. Lamin B1 was also found within the cytoplasm (arrowheads). (I-L) Primary mouse microglia not permeabilized before antibody labeling. (I) Control primary mouse microglia labeled with an antibody for histone H3. (J) Apoptotic primary mouse microglia 3 h after UV irradiation. Patches of anti-histone H3 labeling were detected at the cell surface. (K) Control primary mouse microglia labeled with anti-lamin B1. (L) Apoptotic primary mouse microglia 3 h after UV irradiation labeled with anti-lamin B1. Lamin B1 was exposed at the cell surface. All bars 20 µm.

Supplementary Information
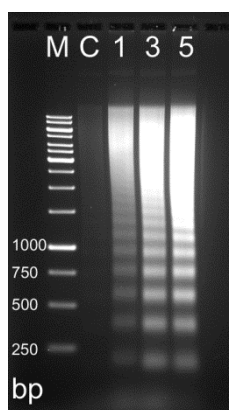
Suppl. Fig. 1

Suppl. Fig. 1 Time course of DNA laddering in BV-2 microglia after UV irradiation. Lane 1: marker (M), Lane 2: control (C); Lane 3-5: DNA of BV-2 cells 1, 3, or 5 h after UV irradiation.

References

1. Kerr JF, Wyllie AH, Currie AR (1972) Apoptosis: a basic biological phenomenon with wide-ranging implications in tissue kinetics. Br J Cancer 26 (4):239-257

2. Rao L, Perez D, White E (1996) Lamin proteolysis facilitates nuclear events during apoptosis. J Cell Biol 135 (6 Pt 1):1441-1455

3. Croft DR, Coleman ML, Li S, Robertson D, Sullivan T, Stewart CL, Olson MF (2005) Actin-myosin-based contraction is responsible for apoptotic nuclear disintegration. J Cell Biol 168 (2):245-255. doi:jcb.200409049 [pii]
10.1083/jcb.200409049

4. Lazebnik YA, Takahashi A, Moir RD, Goldman RD, Poirier GG, Kaufmann SH, Earnshaw WC (1995) Studies of the lamin proteinase reveal multiple parallel biochemical pathways during apoptotic execution. Proc Natl Acad Sci U S A 92 (20):9042-9046

5. Slee EA, Adrain C, Martin SJ (2001) Executioner caspase-3, -6, and -7 perform distinct, non-redundant roles during the demolition phase of apoptosis. J Biol Chem 276 (10):7320-7326. doi:10.1074/jbc.M008363200
M008363200 [pii]

6. Casciola-Rosen LA, Anhalt G, Rosen A (1994) Autoantigens targeted in systemic lupus erythematosus are clustered in two populations of surface structures on apoptotic keratinocytes. J Exp Med 179 (4):1317-1330

7. Radic M, Marion T, Monestier M (2004) Nucleosomes are exposed at the cell surface in apoptosis. J Immunol 172 (11):6692-6700

8. Ravichandran KS (2011) Beginnings of a good apoptotic meal: the find-me and eat-me signaling pathways. Immunity 35 (4):445-455. doi:10.1016/j.immuni.2011.09.004

9. Gaipl US, Munoz LE, Grossmayer G, Lauber K, Franz S, Sarter K, Voll RE, Winkler T, Kuhn A, Kalden J, Kern P, Herrmann M (2007) Clearance deficiency and systemic lupus erythematosus (SLE). J Autoimmun 28 (2-3):114-121. doi:S0896-8411(07)00019-4 [pii]
10.1016/j.jaut.2007.02.005

10. Savill J, Dransfield I, Gregory C, Haslett C (2002) A blast from the past: clearance of apoptotic cells regulates immune responses. Nat Rev Immunol 2 (12):965-975. doi:10.1038/nri957
nri957 [pii]

11. Elliott MR, Ravichandran KS (2010) Clearance of apoptotic cells: implications in health and disease. J Cell Biol 189 (7):1059-1070. doi:jcb.201004096 [pii]
10.1083/jcb.201004096

12. Erwig LP, Henson PM (2007) Immunological consequences of apoptotic cell phagocytosis. Am J Pathol 171 (1):2-8. doi:S0002-9440(10)61936-0 [pii]
10.2353/ajpath.2007.070135

13. Nagata S, Hanayama R, Kawane K (2010) Autoimmunity and the clearance of dead cells. Cell 140 (5):619-630. doi:S0092-8674(10)00129-7 [pii]
10.1016/j.cell.2010.02.014

14. Shao WH, Cohen PL (2011) Disturbances of apoptotic cell clearance in systemic lupus erythematosus. Arthritis research & therapy 13 (1):202. doi:10.1186/ar3206

15. Decker P (2006) Nucleosome autoantibodies. Clin Chim Acta 366 (1-2):48-60. doi:S0009-8981(05)00681-9 [pii]
10.1016/j.cca.2005.11.009

16. Gomez-Puerta JA, Burlingame RW, Cervera R (2008) Anti-chromatin (anti-nucleosome) antibodies: diagnostic and clinical value. Autoimmun Rev 7 (8):606-611. doi:S1568-9972(08)00095-5 [pii]
10.1016/j.autrev.2008.06.005

17. Rumore PM, Steinman CR (1990) Endogenous circulating DNA in systemic lupus erythematosus. Occurrence as multimeric complexes bound to histone. J Clin Invest 86 (1):69-74. doi:10.1172/JCI114716

18. Ramage AE, Fox PT, Brey RL, Narayana S, Cykowski MD, Naqibuddin M, Sampedro M, Holliday SL, Franklin C, Wallace DJ, Weisman MH, Petri M (2011) Neuroimaging evidence of white matter inflammation in newly diagnosed systemic lupus erythematosus. Arthritis Rheum 63 (10):3048-3057. doi:10.1002/art.30458

19. Sciascia S, Bertolaccini ML, Baldovino S, Roccatello D, Khamashta MA, Sanna G (2013) Central nervous system involvement in systemic lupus erythematosus: Overview on classification criteria. Autoimmun Rev 12 (3):426-429. doi:10.1016/j.autrev.2012.08.014

20. Barned S, Goodman AD, Mattson DH (1995) Frequency of anti-nuclear antibodies in multiple sclerosis. Neurology 45 (2):384-385

21. Collard RC, Koehler RP, Mattson DH (1997) Frequency and significance of antinuclear antibodies in multiple sclerosis. Neurology 49 (3):857-861

22. Dore-Duffy P, Donaldson JO, Rothman BL, Zurier RB (1982) Antinuclear antibodies in multiple sclerosis. Arch Neurol 39 (8):504-506

23. Yukitake M, Sueoka E, Sueoka-Aragane N, Sato A, Ohashi H, Yakushiji Y, Saito M, Osame M, Izumo S, Kuroda Y (2008) Significantly increased antibody response to heterogeneous nuclear ribonucleoproteins in cerebrospinal fluid of multiple sclerosis patients but not in patients with human T-lymphotropic virus type I-associated myelopathy/tropical spastic paraparesis. J Neurovirol 14 (2):130-135. doi:790827601 [pii] 10.1080/13550280701883840

24. Comabella M, Rentzsch K, Rio J, Bustamante MF, Borowski K, Stoecker W, Montalban X (2013) Treatment with interferon-beta does not induce anti-nuclear and anti-neuronal serum autoantibodies in multiple sclerosis patients. J Neuroimmunol 255 (1-2):102-104. doi:10.1016/j.jneuroim.2012.10.016

25. Fukazawa T, Kikuchi S, Sasaki H, Hamada K, Hamada T, Miyasaka K, Tashiro K (1997) Anti-nuclear antibodies and the optic-spinal form of multiple sclerosis. Journal of neurology 244 (8):483-488

26. Szmyrka-Kaczmarek M, Pokryszko-Dragan A, Pawlik B, Gruszka E, Korman L, Podemski R, Wiland P, Szechinski J (2012) Antinuclear and antiphospholipid antibodies in patients with multiple sclerosis. Lupus 21 (4):412-420. doi:10.1177/0961203311427550

27. Solomon AJ, Hills W, Chen Z, Rosenbaum J, Bourdette D, Whitham R (2013) Autoantibodies and Sjogren's Syndrome in multiple sclerosis, a reappraisal. PloS one 8 (6):e65385. doi:10.1371/journal.pone.0065385

28. Mecocci P, Ekman R, Parnetti L, Senin U (1993) Antihistone and anti-dsDNA autoantibodies in Alzheimer's disease and vascular dementia. Biological psychiatry 34 (6):380-385

29. Lopez OL, Rabin BS, Huff FJ, Rezek D, Reinmuth OM (1992) Serum autoantibodies in patients with Alzheimer's disease and vascular dementia and in nondemented control subjects. Stroke; a journal of cerebral circulation 23 (8):1078-1083

30. Ginhoux F, Greter M, Leboeuf M, Nandi S, See P, Gokhan S, Mehler MF, Conway SJ, Ng LG, Stanley ER, Samokhvalov IM, Merad M (2010) Fate mapping analysis reveals that adult microglia derive from primitive macrophages. Science 330 (6005):841-845. doi:10.1126/science.1194637

31. Greter M, Merad M (2013) Regulation of microglia development and homeostasis. Glia 61 (1):121-127. doi:10.1002/glia.22408

32. Jung S, Schwartz M (2012) Non-identical twins - microglia and monocyte-derived macrophages in acute injury and autoimmune inflammation. Frontiers in immunology 3:89. doi:10.3389/fimmu.2012.00089

33. Kettenmann H, Hanisch UK, Noda M, Verkhratsky A (2011) Physiology of microglia. Physiol Rev 91 (2):461-553. doi:10.1152/physrev.00011.2010

34. Parkhurst CN, Gan WB (2010) Microglia dynamics and function in the CNS. Curr Opin Neurobiol 20 (5):595-600. doi:S0959-4388(10)00110-8 [pii]
10.1016/j.conb.2010.07.002

35. Graeber MB (2010) Changing face of microglia. Science 330 (6005):783-788. doi:330/6005/783 [pii]
10.1126/science.1190929

36. Polazzi E, Monti B (2010) Microglia and neuroprotection: from in vitro studies to therapeutic applications. Prog Neurobiol 92 (3):293-315. doi:S0301-0082(10)00130-9 [pii]
10.1016/j.pneurobio.2010.06.009

37. Sierra A, Abiega O, Shahraz A, Neumann H (2013) Janus-faced microglia: beneficial and detrimental consequences of microglial phagocytosis. Frontiers in cellular neuroscience 7:6. doi:10.3389/fncel.2013.00006

38. Aguzzi A, Barres BA, Bennett ML (2013) Microglia: scapegoat, saboteur, or something else? Science 339 (6116):156-161. doi:10.1126/science.1227901

39. Rawji KS, Yong VW (2013) The benefits and detriments of macrophages/microglia in models of multiple sclerosis. Clinical & developmental immunology 2013:948976. doi:10.1155/2013/948976

40. Lee P, Lee J, Kim S, Lee MS, Yagita H, Kim SY, Kim H, Suk K (2001) NO as an autocrine mediator in the apoptosis of activated microglial cells: correlation between activation and apoptosis of microglial cells. Brain Res 892 (2):380-385. doi:S0006-8993(00)03257-1 [pii]

41. Ladeby R, Wirenfeldt M, Garcia-Ovejero D, Fenger C, Dissing-Olesen L, Dalmau I, Finsen B (2005) Microglial cell population dynamics in the injured adult central nervous system. Brain Res Brain Res Rev 48 (2):196-206. doi:S0165-0173(04)00186-9 [pii]
10.1016/j.brainresrev.2004.12.009

42. Lee J, Hur J, Lee P, Kim JY, Cho N, Kim SY, Kim H, Lee MS, Suk K (2001) Dual role of inflammatory stimuli in activation-induced cell death of mouse microglial cells. Initiation of two separate apoptotic pathways via induction of interferon regulatory factor-1 and caspase-11. J Biol Chem 276 (35):32956-32965. doi:10.1074/jbc.M104700200
M104700200 [pii]

43. Liu B, Wang K, Gao HM, Mandavilli B, Wang JY, Hong JS (2001) Molecular consequences of activated microglia in the brain: overactivation induces apoptosis. J Neurochem 77 (1):182-189

44. Mayo L, Jacob-Hirsch J, Amariglio N, Rechavi G, Moutin MJ, Lund FE, Stein R (2008) Dual role of CD38 in microglial activation and activation-induced cell death. J Immunol 181 (1):92-103. doi:181/1/92 [pii]

45. Bonetti B, Pohl J, Gao YL, Raine CS (1997) Cell death during autoimmune demyelination: effector but not target cells are eliminated by apoptosis. J Immunol 159 (11):5733-5741

46. Kohji T, Matsumoto Y (2000) Coexpression of Fas/FasL and Bax on brain and infiltrating T cells in the central nervous system is closely associated with apoptotic cell death during autoimmune encephalomyelitis. J Neuroimmunol 106 (1-2):165-171. doi:S0165572800002381 [pii]

47. White CA, McCombe PA, Pender MP (1998) Microglia are more susceptible than macrophages to apoptosis in the central nervous system in experimental autoimmune encephalomyelitis through a mechanism not involving Fas (CD95). Int Immunol 10 (7):935-941

48. Ransohoff RM, Engelhardt B (2012) The anatomical and cellular basis of immune surveillance in the central nervous system. Nat Rev Immunol 12 (9):623-635. doi:10.1038/nri3265

49. Chastain EM, Duncan DS, Rodgers JM, Miller SD (2011) The role of antigen presenting cells in multiple sclerosis. Biochim Biophys Acta 1812 (2):265-274. doi:S0925-4439(10)00145-6 [pii]
10.1016/j.bbadis.2010.07.008

50. Goverman JM (2011) Immune tolerance in multiple sclerosis. Immunol Rev 241 (1):228-240. doi:10.1111/j.1600-065X.2011.01016.x

51. Frisoni L, McPhie L, Colonna L, Sriram U, Monestier M, Gallucci S, Caricchio R (2005) Nuclear autoantigen translocation and autoantibody opsonization lead to increased dendritic cell phagocytosis and presentation of nuclear antigens: a novel pathogenic pathway for autoimmunity? J Immunol 175 (4):2692-2701. doi:175/4/2692 [pii]

52. Frisoni L, McPhie L, Kang SA, Monestier M, Madaio M, Satoh M, Caricchio R (2007) Lack of chromatin and nuclear fragmentation in vivo impairs the production of lupus anti-nuclear antibodies. J Immunol 179 (11):7959-7966. doi:179/11/7959 [pii]

53. Gabler C, Blank N, Hieronymus T, Schiller M, Berden JH, Kalden JR, Lorenz HM (2004) Extranuclear detection of histones and nucleosomes in activated human lymphoblasts as an early event in apoptosis. Ann Rheum Dis 63 (9):1135-1144. doi:10.1136/ard.2003.011452
63/9/1135 [pii]

54. Konishi A, Shimizu S, Hirota J, Takao T, Fan Y, Matsuoka Y, Zhang L, Yoneda Y, Fujii Y, Skoultchi AI, Tsujimoto Y (2003) Involvement of histone H1.2 in apoptosis induced by DNA double-strand breaks. Cell 114 (6):673-688. doi:S0092867403007190 [pii]

55. Okamura H, Yoshida K, Amorim BR, Haneji T (2008) Histone H1.2 is translocated to mitochondria and associates with Bak in bleomycin-induced apoptotic cells. J Cell Biochem 103 (5):1488-1496. doi:10.1002/jcb.21537

56. Schiller M, Bekeredjian-Ding I, Heyder P, Blank N, Ho AD, Lorenz HM (2008) Autoantigens are translocated into small apoptotic bodies during early stages of apoptosis. Cell Death Differ 15 (1):183-191. doi:4402239 [pii]
10.1038/sj.cdd.4402239

57. Zierler S, Klein B, Furtner T, Bresgen N, Lütz-Meindl U, Kerschbaum HH (2006) Ultraviolet irradiation-induced apoptosis does not trigger nuclear fragmentation but translocation of chromatin from nucleus into cytoplasm in the microglial cell-line, BV-2. Brain Res 1121 (1):12-21. doi:S0006-8993(06)02635-7 [pii]
10.1016/j.brainres.2006.08.122

58. Blasi E, Barluzzi R, Bocchini V, Mazzolla R, Bistoni F (1990) Immortalization of murine microglial cells by a v-raf/v-myc carrying retrovirus. J Neuroimmunol 27 (2-3):229-237

59. Giulian D, Baker TJ (1986) Characterization of ameboid microglia isolated from developing mammalian brain. J Neurosci 6 (8):2163-2178

60. Frei K, Bodmer S, Schwerdel C, Fontana A (1986) Astrocyte-derived interleukin 3 as a growth factor for microglia cells and peritoneal macrophages. J Immunol 137 (11):3521-3527

61. Lütz-Meindl U, Aichinger N (2004) Use of energy-filtering transmission electron microscopy for routine ultrastructural analysis of high-pressure-frozen or chemically fixed plant cells. Protoplasma 223:155-162. doi:10.1007/s00709-003-0033-3

62. Brack K, Frings W, Dotzauer A, Vallbracht A (1998) A cytopathogenic, apoptosis-inducing variant of hepatitis A virus. J Virol 72 (4):3370-3376

63. Batista LF, Kaina B, Meneghini R, Menck CF (2009) How DNA lesions are turned into powerful killing structures: insights from UV-induced apoptosis. Mutat Res 681 (2-3):197-208. doi:S1383-5742(08)00136-1 [pii]
10.1016/j.mrrev.2008.09.001

64. Ferrando-May E, Cordes V, Biller-Ckovric I, Mirkovic J, Gorlich D, Nicotera P (2001) Caspases mediate nucleoporin cleavage, but not early redistribution of nuclear transport factors and modulation of nuclear permeability in apoptosis. Cell Death Differ 8 (5):495-505. doi:10.1038/sj.cdd.4400837

65. Faleiro L, Lazebnik Y (2000) Caspases disrupt the nuclear-cytoplasmic barrier. J Cell Biol 151 (5):951-959

66. Bano D, Dinsdale D, Cabrera-Socorro A, Maida S, Lambacher N, McColl B, Ferrando-May E, Hengartner MO, Nicotera P (2010) Alteration of the nuclear pore complex in Ca(2+)-mediated cell death. Cell Death Differ 17 (1):119-133. doi:cdd2009112 [pii] 10.1038/cdd.2009.112

67. Patre M, Tabbert A, Hermann D, Walczak H, Rackwitz HR, Cordes VC, Ferrando-May E (2006) Caspases target only two architectural components within the core structure of the nuclear pore complex. J Biol Chem 281 (2):1296-1304. doi:10.1074/jbc.M511717200

68. Gilthorpe JD, Oozeer F, Nash J, Calvo M, Bennett DL, Lumsden A, Pini A (2013) Extracellular histone H1 is neurotoxic and drives a pro-inflammatory response in microglia. F1000Research 2. doi:10.12688/f1000research.2-148.v1

69. Knight JS, Carmona-Rivera C, Kaplan MJ (2012) Proteins derived from neutrophil extracellular traps may serve as self-antigens and mediate organ damage in autoimmune diseases. Frontiers in immunology 3:380. doi:10.3389/fimmu.2012.00380

70. Kaplan MJ, Radic M (2012) Neutrophil extracellular traps: double-edged swords of innate immunity. J Immunol 189 (6):2689-2695. doi:10.4049/jimmunol.1201719

71. Darrah E, Andrade F (2012) NETs: the missing link between cell death and systemic autoimmune diseases? Frontiers in immunology 3:428. doi:10.3389/fimmu.2012.00428

72. Mantovani A, Cassatella MA, Costantini C, Jaillon S (2011) Neutrophils in the activation and regulation of innate and adaptive immunity. Nat Rev Immunol 11 (8):519-531. doi:10.1038/nri3024

73. Brinkmann V, Zychlinsky A (2012) Neutrophil extracellular traps: is immunity the second function of chromatin? J Cell Biol 198 (5):773-783. doi:10.1083/jcb.201203170

74. Goldmann O, Medina E (2012) The expanding world of extracellular traps: not only neutrophils but much more. Frontiers in immunology 3:420. doi:10.3389/fimmu.2012.00420

75. Amulic B, Hayes G (2011) Neutrophil extracellular traps. Curr Biol 21 (9):R297-298. doi:10.1016/j.cub.2011.03.021

76. Brinkmann V, Reichard U, Goosmann C, Fauler B, Uhlemann Y, Weiss DS, Weinrauch Y, Zychlinsky A (2004) Neutrophil extracellular traps kill bacteria. Science 303 (5663):1532-1535. doi:10.1126/science.1092385

77. Yousefi S, Simon D, Simon HU (2012) Eosinophil extracellular DNA traps: molecular mechanisms and potential roles in disease. Curr Opin Immunol 24 (6):736-739. doi:10.1016/j.coi.2012.08.010

78. von Kockritz-Blickwede M, Goldmann O, Thulin P, Heinemann K, Norrby-Teglund A, Rohde M, Medina E (2008) Phagocytosis-independent antimicrobial activity of mast cells by means of extracellular trap formation. Blood 111 (6):3070-3080. doi:10.1182/blood-2007-07-104018

79. Chow OA, von Kockritz-Blickwede M, Bright AT, Hensler ME, Zinkernagel AS, Cogen AL, Gallo RL, Monestier M, Wang Y, Glass CK, Nizet V (2010) Statins enhance formation of phagocyte extracellular traps. Cell Host Microbe 8 (5):445-454. doi:10.1016/j.chom.2010.10.005

80. Aulik NA, Hellenbrand KM, Czuprynski CJ (2012) Mannheimia haemolytica and its leukotoxin cause macrophage extracellular trap formation by bovine macrophages. Infect Immun 80 (5):1923-1933. doi:10.1128/IAI.06120-11

81. Hellenbrand KM, Forsythe KM, Rivera-Rivas JJ, Czuprynski CJ, Aulik NA (2013) Histophilus somni causes extracellular trap formation by bovine neutrophils and macrophages. Microbial pathogenesis 54:67-75. doi:10.1016/j.micpath.2012.09.007

82. Mohanan S, Horibata S, McElwee JL, Dannenberg AJ, Coonrod SA (2013) Identification of macrophage extracellular trap-like structures in mammary gland adipose tissue: a preliminary study. Frontiers in immunology 4:67. doi:10.3389/fimmu.2013.00067

83. Wong KW, Jacobs WR, Jr. (2013) Mycobacterium tuberculosis exploits human interferon gamma to stimulate macrophage extracellular trap formation and necrosis. The Journal of infectious diseases 208 (1):109-119. doi:10.1093/infdis/jit097

84. Hirsch JG (1958) Bactericidal action of histone. J Exp Med 108 (6):925-944

85. Parseghian MH, Luhrs KA (2006) Beyond the walls of the nucleus: the role of histones in cellular signaling and innate immunity. Biochem Cell Biol 84 (4):589-604. doi:o06-082 [pii] 10.1139/o06-082

86. Yipp BG, Petri B, Salina D, Jenne CN, Scott BN, Zbytnuik LD, Pittman K, Asaduzzaman M, Wu K, Meijndert HC, Malawista SE, de Boisfleury Chevance A, Zhang K, Conly J, Kubes P (2012) Infection-induced NETosis is a dynamic process involving neutrophil multitasking in vivo. Nat Med 18 (9):1386-1393. doi:10.1038/nm.2847

87. Fuchs TA, Abed U, Goosmann C, Hurwitz R, Schulze I, Wahn V, Weinrauch Y, Brinkmann V, Zychlinsky A (2007) Novel cell death program leads to neutrophil extracellular traps. J Cell Biol 176 (2):231-241. doi:10.1083/jcb.200606027

88. Yousefi S, Gold JA, Andina N, Lee JJ, Kelly AM, Kozlowski E, Schmid I, Straumann A, Reichenbach J, Gleich GJ, Simon HU (2008) Catapult-like release of mitochondrial DNA by eosinophils contributes to antibacterial defense. Nat Med 14 (9):949-953. doi:10.1038/nm.1855

89. Yousefi S, Mihalache C, Kozlowski E, Schmid I, Simon HU (2009) Viable neutrophils release mitochondrial DNA to form neutrophil extracellular traps. Cell Death Differ 16 (11):1438-1444. doi:10.1038/cdd.2009.96

90. Senecal JL, Rauch J, Grodzicky T, Raynauld JP, Uthman I, Nava A, Guimond M, Raymond Y (1999) Strong association of autoantibodies to human nuclear lamin B1 with lupus anticoagulant antibodies in systemic lupus erythematosus. Arthritis Rheum 42 (7):1347-1353. doi:10.1002/1529-0131(199907)42:7<1347::AID-ANR7>3.0.CO;2-#

91. Dieude M, Senecal JL, Rauch J, Hanly JG, Fortin P, Brassard N, Raymond Y (2002) Association of autoantibodies to nuclear lamin B1 with thromboprotection in systemic lupus erythematosus: lack of evidence for a direct role of lamin B1 in apoptotic blebs. Arthritis Rheum 46 (10):2695-2707. doi:10.1002/art.10552

92. Moisan E, Girard D (2006) Cell surface expression of intermediate filament proteins vimentin and lamin B1 in human neutrophil spontaneous apoptosis. J Leukoc Biol 79 (3):489-498. doi:10.1189/jlb.0405190